Impact of W events and dust on JET-ILW operation

M.Sertoli[a*], J.C. Flanagan[b], M. Bacharis[c], O. Kardaun[a], A. Jarvinen[d], G.F. Matthews[b], S. Brezinsek[e], D. Harting[b], A. Cackett[b], E. Hodille[b], I.H. Coffey[f], E. Lazzaro[g], T. Pütterich[a] and JET-EFDA Contributors[#]

JET-EFDA Culham Science Centre, Abington, OX14 3DB, UK

[a] *Max-Planck-Institut für Plasmaphysik, 85748 Garching, Germany*

[b] *CCFE Fusion Association, Culham Science Centre, Abingdon, OX14 3DB, UK*

[c] *Blackett Laboratory, Imperial College London, Prince Consort Road, London, UK*

[d] *Aalto University, Association Tekes, Espoo, Finland*

[e] *Forschungszentrum Juelich GmbH, EURATOM Association, 52425 Juelich, Germany*

[f] *Queen's University, Belfast, BT7 1NN, UK*

[g] *Istituto di Fisica del Plasma C.N.R., Milan, Italy*

[#] *See the Appendix of F. Romanelli et al., Proceedings of the 24th IAEA Fusion Energy Conference 2012, San Diego, US*

Abstract

The occurrence of transient impurity events (TIE) leading to intense radiation spikes in JET plasma discharges has been studied since the installation of the ITER-like Wall (ILW). To generate the observed average increase in radiated power of 1.5 MW, a spherical particle of solid W of radius > 90 μm would be required. The drop in plasma energy caused by W-TIEs is fully recovered in 90% of all cases, only 1% inducing a longer term loss in plasma energy which sometimes leads to the shut-down of plasma operation. TIEs are correlated with disruptions and with measurements of the dust mobilized by disruptions using the high resolution Thomson scattering (HRTS) diagnostic. The dust characteristics giving rise to TIEs have been studied using the dust transport code DTOKS and the 1D impurity transport code STRAHL.

PACS: 52.25.Vy, 52.70.Kz, 52.40.Hf, 52.55.Fa

PSI-20 Keywords: Dust, Impurity, ILW, Radiation, Tungsten

Corresponding author address: Boltzmannstrasse 2, 85748 Garching, Germany

Corresponding author e-mail: marco.sertoli@ipp.mpg.de

Presenting author: Marco Sertoli

Presenting author e-mail: marco.sertoli@ipp.mpg.de

1. Introduction

The understanding of dust production, control and its effects on plasma operation is a major concern not only for future tokamaks such as ITER, but also for present-day devices such as JET (see e.g. [1, 2, 3, 4, 5] and references therein). Transient impurity events (TIEs, also called UFOs), visible as sharp increases in the total radiated power (figure 1b) similar to what caused by laser ablation experiments, have the potential to terminate the discharge due to extreme radiation losses in JET.

This contribution reports on the study of TIEs observed in JET since the installation of the ITER-like wall (ILW), on their impact on regular plasma operation and their relation to dust. The responsible impurities have been studied using vacuum-ultra-violet (VUV) spectroscopy. Their occurrence has been correlated with plasma geometry, arcs from lower-hybrid (LH) antennas, reciprocating probe (RCP) plunges and laser blow-off (LBO) (section 2). Correlation analysis with plasma parameters has been performed (section 3) and comparison with independent estimates on the dust mobilized by the disruptions obtained using the high resolution Thomson scattering (HRTS) diagnostic and correlation with disruption occurrence is reported (section 4). The limited amount of TIE-induced disruptions are not reported since they have been intensively analysed elsewhere (see e.g. [6]). Modelling of the particle ablation has been

performed using the dust code DTOKS [7]. The 1D impurity transport code STRAHL [8] has been employed to estimate the parameters of the dust particles which could lead to the observed increases in radiated power (section 5). A discussion and conclusions are given in section 6.

2. TIE identification and geometrical dependencies

The occurrence of TIEs has been analysed in all JET pulse number (JPN) in range $80128 - 85699$ with plasma current $I_p > 1$ (MA). A total of 3388 events have been detected in 4144 discharges (~ 23 h of plasma), for an average of 1 event every 25 seconds of plasma. For each event, a database has been built with the responsible impurities, the maximum excursion in total radiated power and drop in plasma energy due to the event. The plasma current, plasma energy, ohmic and externally applied heating powers, radiated power, line averaged electron density, geometrical parameters (distance form inner and outer limiter, strike-point configuration, elongation, triangularity, volume), the vacuum toroidal magnetic field, q_{95} as well as confinement factors ($H89$ and $H98(y.2)$) and the Greenwald fraction have also been tabulated for correlation purposes.

A second database using the same selection criteria containing the total plasma operation time (in steps of 10 ms) for each quantity contained in the database has been used as normalization factor for the number of events. The result is a TIE rate (# of events / operation time = Hz), its error bar evaluated propagating the statistical error of the number of events, equal to its square root.

2.1. Responsible Impurities

The VUV-spectrometers used for this study can distinguish Ni, Fe, Cr, Cu, Al and W spectral features [9] and the events have been divided in three element groups:

i) ***W*** (51% of all events): events where W is detected (usually alone).

ii) ***Ni/Fe/Cr*** (26%): events where either Ni, Fe or Cr are visible (usually in paris or triples, from either Inconel structural material or steel support structures).

iii) ***Others*** (27%): events where either Al or Cu are observed ($< 1\%$) or no responsible impurity can be identified.

An example of the time evolution of the line intensities of W, Ni and Fe is given in figure 1 for two unidentified and one (the last one) W event.

For about 10% of the W events either Ni, Fe or Cr have also been detected. This can be understood since the ILW includes PFCs of different material mixtures (bulk W, W-coated CFC, Be-coated Inconel, bulk Be [10]) and the dust particles involved may contain a combination of them. The robustness of the rationale behind the element groups is anyway confirmed by those TIEs induced by LH-arcs, RCP plunges and LBO injections. 5 TIEs have been found to correlate with LH-arcs (out of 19 arcs occurring in the time-range of interest) and the 22 events correlating with RCP plunges (out of a total of 217 plunges) are dominated by *Ni/Fe/Cr*, consistent with the material of the LH-launcher (stainless steel) and of the probe shaft (Inconel / steel). The 41 events which correlate with LBO injections (out of a total of 55 LBOs) show an element distribution which is consistent with the injected materials: 38% Ni, 18% W and 44% Mo or Zr, the latter two included in the *Others* group defined above since not detected by the VUV spectrometers used. The analysis presented from now on excludes the events listed above and concentrates on the 3320 events whose direct cause could not been determined.

2.2. Geometrical dependencies

The probability of TIEs occurring in limited plasmas is very low, only 8% of all the detected events taking place over the $\sim 7\ h$ of limited-plasma operation (table 1). Most events occur in diverted configurations, exhibiting a 57 mHz rate if the outer strike-point is on a horizontal tile while drops to $< 1\ mHz$ If the outer strike-point is on a vertical tile. This difference can be interpreted noting that the horizontal part of the divertor is a deposition zone for material coming from the main chamber. Dust accumulating here may then be mobilized by transient heat and particle loads (e.g. ELMs) or thermal stresses leading to the observed TIEs.

3. Impact on plasma operation and parametric dependencies

Throughout the ILW campaigns, a limited number of TIEs lead to pulse termination due to extreme radiation losses leading to a collapse of the temperature profiles (e.g. the W event in JPN 81765 at $\sim 10.5\ s$). To investigate the effect of such each event on the background plasma, the loss in plasma energy (e.g. in figure 1a) and its recovery within $\sim 600\ ms$ has been tabulated. Only those events occurring at plasma equilibrium with stationary plasma energy before the occurrence of the event and with stable plasma current and additional heating within $\sim 600\ ms$ from the event (as e.g. the 2^{nd} and 3^{rd} events in figure 1) have been considered so to be sure to detect the effects of TIEs and not those caused or masked by evolving plasma background. Events occurring within few hundred milliseconds from one another have also been neglected restricting the analysis to the effects due to single events. Assuming this sub-set is representative of the whole database, the conditional probability of an event of a specific element group leading to a detectable long term percentage loss in plasma energy δW_P with respect to the value before the event occurred W_P is shown in figure 2 and summarized in table 2.

The plasma recovers completely or exhibits a minor long-term loss in 89% of all cases. W particles are clearly the most *dangerous*, 10% of all events leading to moderate losses and, in 1% of all cases to extreme losses $> 60\%$. If all of the latter events were to lead to the termination of the plasma, this would translate in a 0.8% *TIE-induced* plasma termination rate. This is a factor 4 lower than the unintentional disruption rate observed in the last years of JET-C (3.4%) and an order of magnitude lower than the rate observed in the 2011-2012 JET-ILW campaigns (10%) [6].

3.1. Parametric dependencies

The parameter space within which TIEs occur is broadly populated and no clear scenario of highest TIE-rate has yet been found for the current data-set. To analyse this issue further we start by looking at univariate distributions which clearly show that the rate increases with: (i) gas puff rate Φ_D $(el.\ s^{-1})$; (ii) upper triangularity δ_u; (iii) closeness of the plasma to the inner wall $R_{in} - R_{wall,in}$ (m) (where R_{in} and $R_{wall,in}$ are the major radius of the last-closed-flux-surface (LCFS) and of inner wall at $z = 0$ respectively); (iv) total heating power normalized to the L-H power threshold scaling P_{heat}/P_{thr} (see [11] for P_{thr} formula). These trends are confirmed by multiple regression analysis which we performed by employing SAS PROC LOGISTIC [12, 13, 14]. This procedure applies a log-linear model for $log(P/(1-P))$ in terms of the plasma parameters on a logarithmic scale and assumes binomial distributions of the number of events (TIEs) for fixed values of the plasma parameters.

For this analysis, a sub-set of the original database has been used according to the following selection rules: (i) lower-single-null (LSN) discharges; (ii) flat top phases $(\delta I_P/I_P < 1\%)$ with $I_P > 1\ MA$; (iii) stationarity $(|\delta P_{ext}/P_{ext}| < 5\%$, $|\delta \langle n_e \rangle / \langle n_e \rangle| < 5\%$ and $-0.05 < \langle (dW_{DIA}/dt)/W_{DIA} \rangle < 0.35)$. Here, I_P is the plasma current, P_{ext} the external heating power, $\langle n_e \rangle$ the line averaged electron density, W_{DIA}

the diamagnetic energy. All quantities have been interpolated on a time axis with 50 ms time resolution and averaged over 500 ms. The response function for the regression has been set such that it takes a value of 1 if at least one event occurs in the 500 ms time bin or 0 if no event takes place. Omitting 19 discharges were gas puff rate data was missing, this standard sub-set contains both L- and H-modes and consists of 2933 discharges for a total of 25758 operational time-bins of which 273 ($\sim 1\%$) show the occurrence of one or more events.

The results (equation 1) show the same trends of the univariate distributions and in addition provide quantitative information on the joint effects of the different plasma parameters on the probability of TIE occurrence while keeping constant all other parameters present in the formula:

$$\begin{aligned} log\left(\frac{P}{1-P}\right) = -8.1 + (3.5 \pm 2.4) \cdot log(\delta_u + 1) + \\ (-1.1 \pm 0.6) \cdot (R_{in} - R_{wall,in}) + \\ (0.33 \pm 0.12) \cdot \Phi_D + \\ (0.43 \pm 0.24) \cdot (P_{heat}/P_{thr}) \end{aligned} \quad (1)$$

The errors indicate twice the estimated standard deviation of the estimated regression coefficients. Other plasma parameters (such as distance from the outer wall $R_{wall,out} - R_{out}$, plasma current I_P, safety factor q_{95} and confinement scaling factors $H89$ and $H98(y,2)$) have been considered, but did not have a statistically significant effect on the TIE probability (according to the criterion that their 95 % estimated confidence intervals included the hypothesis of zero effect) and were therefore omitted from the regression analysis. Furthermore, when separately analysing L- and H-mode subsets classifying them on both H-mode and power threshold scaling factors, no appreciable difference in the logistic regression was found.

Provided the model with the selected variables is to a reasonable approximation correct, the degree with which the regression variables can affect the probability (at constant values of the other parameters) can be quantified by evaluating the probability variation over the range spanned by the regression variables. On the logistic scale $log(P/(1-P))$, this is calculated by multiplying the regression coefficient by 5 times the sample standard deviation (SD) of the regression variables. Denoting the regression coefficient of e.g. Φ_D by $\hat{\alpha}_{\Phi_D}$, this translates to $|\hat{\alpha}_{\Phi_D} \cdot 5\, SD(log(\Phi_D))|$. For the different regression variables, the values of these probability ranges on logistic scale are: $(\delta_u + 1) \rightarrow 0.97$, $(R_{in} - R_{wall,in}) \rightarrow 1.65$, $\Phi_D \rightarrow 2.0$, $P_{heat}/P_{thr} \rightarrow 1.44$. In order of importance, the total gas puff rate has the largest impact on the TIE probability, exhibiting about a factor 2 higher range than the upper triangularity, while the distance from the inner wall and normalized heating power occupy an intermediate position between these two extremes.

4. Correlation with disruptions

If disruptions and TIEs were cause-effect related, one would expect TIEs to occur more often either in discharges following a disruption or in discharges approaching a disruption. Within 4 plasma discharges after a disruption the rate is 50% higher than the 40 mHz average while for events occurring further away the value is 25% lower. In order to account for possible *cumulative* effects due to disruptions occurring in subsequent discharges or few discharges from one another, the events have been re-binned accounting only for those events occurring a sufficient number of plasma discharges after the $2^{nd} - last$ disruption. Whether all discharges are accounted for or whether only those occurring 10, 20 or 30 plasma discharges after the $2^{nd} - last$ disruption are considered, the decreasing trend is still observed.

No relation of such kind has instead been found when correlating the TIE-rate to the number of discharges approaching a disruption. It can therefore be clearly stated that TIEs do not have a direct effect on disruptions, but that disruptions have an effect on the TIE rate. This could be due either to a redistribution of particles onto more accessible areas of the machine or through a generation of particles.

4.1. Comparison with HRTS dust data

The time evolution of the TIE rate has been correlated with estimates of the dust mobilized by disruptions determined by particle scattering (Rayleigh, Mie etc.) recorded with the HRTS diagnostic system [15, 16]. The HRTS detects only particles passing the laser beam (1064 nm, 5 J, 20 ns pulses, 20 Hz) during the $1-2$ s after the current quench, so only a small fraction of the particles present in the machine is covered. Since TIEs are detected during the plasma discharge, in order to compare these two data-sets only the events occurring within 5 discharges after the last disruption have been considered. The bins have been kept rather large (350 plasma discharges) to ensure a relevant number of disruptions in each bin.

The fine structure of the temporal evolution of the TIE-rate (black bars in figure 3) is qualitatively well reproduced by the rate of HRTS dust events normalized to the number of disruptions (green). The large drop in rate occurring in the first $\sim$ 1400 discharges is seen by both analysis by a similar factor (TIEs falling of a factor 2.5, HRTS of a factor 3.3) and an increase in rate is seen by both methods at the bin centered at $JPN \sim 81713$. The strong increase in HRTS rate at the end of the analysed range has been found to correlate with a malfunctioning of the reciprocating probe which lead to debris falling from the probe into the vacuum vessel, starting at JPN 84747 (third-last bin in figure 3) and ending with the probe head falling into the vacuum vessel during JPN 85484 (last bin). Since the HRTS diagnostic and the RCP are located in the same

octant, the large number of events detected are most probably directly caused by these debris passing through the line-of-sights of the diagnostic and which not necessarily are subsequently detected as TIEs [17].

5. Modelling of TIEs

Modelling of dust trajectory and ablation has been undertaken using the code DTOKS. The physical model includes charging and heating of the dust particle, and the equation of motion accounts for the Lorentz force, ion drag and gravity. The particles are assumed of spherical shape and the composition, size, initial velocity and injection angles are input parameters. The background plasma has been taken from an EDGE2D-Eirene simulation [18] of JPN 82550 in time range $[15, 16]$ s. Scans in particle size ($r = [10, 100]$ μm) and in injection angle ($\phi = [-90, +90]$ deg) of a W particle originating from the outer strike-point position with injection velocity of 10 m/s will be discussed here.

Figure 4 displays the poloidal cross-section of the plasma, showing the position of ablation of a W particle along its flight path. The different colours correspond to different particle sizes (see figure caption). The larger the particle mass the deeper inside the plasma core it will ablate, but the ratio between the total injected mass and the mass ablated (*screening factor*) reaches a plateau value of $\sim 50\%$ for particle sizes above 20 (μm). Shielding of the dust particle [5] by the ablation cloud is not accounted for.

For the particles reaching the plasma core, the 1D impurity transport code STRAHL has been used to simulate the observed increase in total radiated power caused by TIEs. The perpendicular transport in the SOL and core plasma is simulated using a diffusive and convective ansatz. The diffusion has been set to *typical* values observed in fusion

devices: 0.5 (m^2/s) in the SOL, 3 (m^2/s) at the pedestal top, decaying to 0.5 (m^2/s) in the plasma centre. The convection velocity was chosen for constant equilibrium impurity concentration (i.e. $-v/D = \nabla n_e/n_e$). Recycling at the wall has been switched off, imposing the condition that the particles do not re-enter the plasma the moment they reach the wall. The main plasma parameters have been taken from the EDGE2D-Eirene simulations used for the DTOKS runs. Since the DTOKS simulations lead to a maximum $\sim 4\ cm$ penetration inside the separatrix for particles $> 25\ \mu m$, the source position has been set to a representative but conservative value of $r - r_{LCFS} = -1.5\ (cm)$ inside the separatrix.

The number of ablated ions needed to generate the observed average increase in radiated power is of the order of $2 \cdot 10^{17}$ which leads to a minimum initial particle size of $\sim 90\ \mu m$. This is of the order of the estimated size of the W droplets released during the bulk-W melt experiments [19]. On the other hand, this value is a lower estimate since it does not account for screening effects, e.g. its ablation in the SOL or its redeposition on the walls. If only 50% or 10% of its mass were to reach the plasma core, the original particle size would increase to $\sim 115\ \mu m$ or $\sim 200 \mu m$ respectively.

In order to account for the varying plasma parameters in which the TIEs have been observed to occur, an independent estimate of the minimum particle size has been performed: by using the experimental temperature and density profiles from HRTS for each event and assuming local-ionization-equilibrium for the radiation modelling, the minimum particle size is $\sim 70\ \mu m$, slightly smaller but of the same order of the estimate from the transport calculations. Using this last number and accounting for the total number of detected W-events (1697), 0.07 g of W dust is needed to generate them. If screening factors of 50% or 10% are considered, this value increases to 0.14 g or 0.74 g respectively.

6. Discussion and conclusions

The occurrence of transient impurity events has been studied in JET-ILW analysing their impact on plasma operation and correlating their rate with plasma parameters, disruptions and independent estimates on dust mobilized by disruptions using the HRTS diagnostic.

The excellent correlation between the time evolution of the TIE rate and the dust events detected by the HRTS diagnostic confirms the assumption that TIEs are caused by dust particles. A general decreasing trend of both quantities suggests that the amount of dust in JET-ILW is decreasing with time and the rate of particle-creation appears to be lower than that of its destruction. Disruptions are found to have an enhancing effect on the TIE rate which increases by a factor 1.5 with respect to the average value in discharges following a disruption. It is still not clear if this is because disruptions create particles or merely redistribute them onto more accessible parts of the torus.

Less than 1% of all TIEs have caused a long term loss in plasma energy which have sometimes led to discharge termination. This translates in a rate of TIE-induced plasma termination *risk* of 0.8%, much lower than the unintentional disruption rate in both JET-C and JET-ILW. The minimum particle size that could lead to the observed increase in radiated power is $\sim 70 - 90\ \mu m$, of the same order as what estimated from the W melt experiments [19]. The W-coated CFC tiles probably the origin of the W dust since delaminations have been observed on several tiles [20]. For future machines such as ITER it is important to understand this so to optimize the design of the plasma facing components.

Future studies should include the effects of ELMs since they could lead to the initial mobilization of the dust. Experimental effort should be dedicated to constrain modelling parameters so to better understand the physical processes at play. A benchmarking

between two different dust-transport codes (DTOKS [7] and DUSTTRACK [21]) has already started.

Acknowledgments

This work was supported by EURATOM and carried out within the framework of the European Fusion Development Agreement. The views and opinions expressed herein do not necessarily reflect those of the European Commission.

References

[1] Federici G *et al* 2001 *Nuclear Fusion* **41** 1967

[2] Winter J 2004 *Plasma Physics and Controlled Fusion* **46** B583

[3] Rudakov D L *et al* 2008 *Review of Scientific Instruments* **79** 10F303

[4] Roth J *et al* 2009 *Journal of Nuclear Materials* **390-391** 1 – 9

[5] Krasheninnikov S I *et al* 2011 *Plasma Physics and Controlled Fusion* **53** 083001

[6] de Vries P C *et al* 2014 *Physics of Plasmas* **21** 056101

[7] Bacharis M *et al* 2010 *Physics of Plasmas* **17** 042505

[8] Dux R STRAHL User Manual Laborbericht 10/30, IPP Garching, September 2006

[9] Sertoli M *et al* 2014 *Physica Scripta* **2014** 014014

[10] Matthews G 2013 *Journal of Nuclear Materials* **438, Supplement** S2 – S10

[11] Snipes J A *et al* 2000 *Plasma Physics and Controlled Fusion* **42** A299

[12] SAS Institute Inc. 2012. SAS/IML12.1 Users Guide. Cary, NC: SAS Institute Inc.

[13] Schmitz P M I Logistic regression in medical decision making and epidemiology

[14] Hosmer D W *et al* *Applied Logistic Regression* Wiley, 3rd edition, 2013

[15] Pasqualotto R *et al* 2004 *Review of Scientific Instruments* **75** 3891–3893

[16] Giovannozzi E *et al* 2010 *Review of Scientific Instruments* **81** 10E131

[17] Flanagan J Invited I4.114 EPS 2014 Invited, Submitted to *Plasma Physics and Controlled Fusion*

[18] Järvinen A Invited I18 PSI 2014, Submitted to *Journal of Nuclear Materials*

[19] Coenen J Invited I8 PSI 2014, Submitted to *Journal of Nuclear Materials*

[20] Widdowson A *et al* 2014 *Physica Scripta* **2014** 014010

[21] Lazzaro E *et al* 2012 *Plasma Physics and Controlled Fusion* **54** 124043

Table captions

1) Total plasma time (h), number of events, event frequency (mHz) and most probable element for limited (*Limiter*) and diverted configurations with the outer strike-point on a horizontal target plate (*Horiz. Outer SP*) or on a vertical one (*Vert. Outer SP*)

2) Long-term ($> 600\ ms$) percentage loss in plasma energy for the different element groups.

Tables

	Total plasma time	Number of events	Event rate	Most abundant element
	(h)		(mHz)	(% in that configuration)
Limiter	6.8	260	10	$Ni/Fe/Cr$ (50 %)
Horiz. Outer SP	14.6	3047	57	W (55 %)
Vert. Outer SP	1.7	4	< 1	-

Table 1.

	Minor loss $\delta W/W < 10\%$	Moderate loss $10 < \delta W/W < 30\%$	Extreme loss $\delta W/W > 60\%$
	(% of events)	(% of events)	(% of events)
W	86	10	1
$Ni/Fe/Cr$	94	5	< 1
$Others$	92	5	1
total	89	7	1

Table 2.

Figure captions

1) Example of TIEs occurring in JPN 81611: (a) plasma current and plasma energy; (b) NBI and radiated power; (c) VUV signals for W, Ni and Fe. Colour coding as in label.

2) Conditional probability of an event leading to certain percentage loss in plasma energy 200 ms after the event (0% = full recovery, 100% = complete loss). W in black, $Ni/Fe/Cr$ in red, $Others$ in blue.

3) TIE-rate evolution in time (black bars) and HRTS number of dust events (green) vs. discharge number. The white and green numbers on the graph give the number of TIEs and the number of disruptions in each bin respectively. Red circles highlight possible outliers in the HRTS data.

4) Poloidal cross-section of plasma discharge JPN 82550 at 15.5 seconds. Coloured regions in the divertor indicate the average ablation position for DTOK results for spherical W particles of radius 100 μm (blue), 75 μm (lilac), 50 μm (red), 25 μm (green) and 10 μm (orange).

Figures

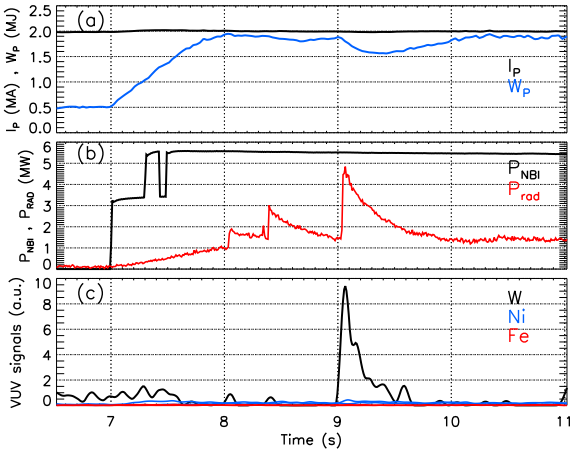

Figure 1.

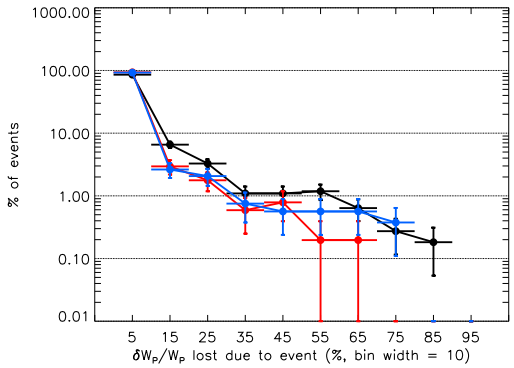

Figure 2.

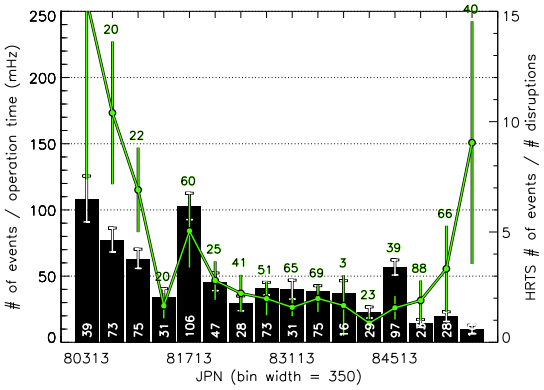

Figure 3.

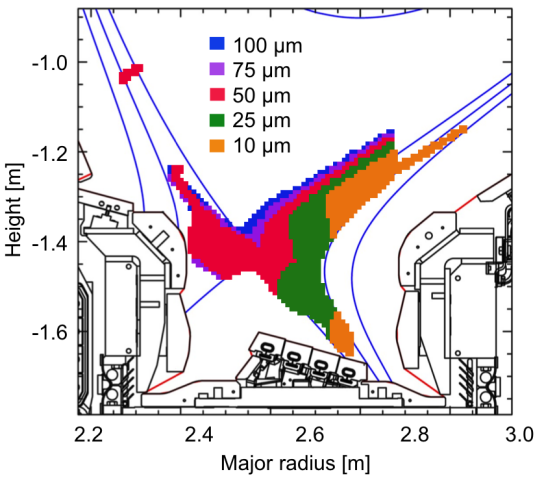
100 µm
75 µm
50 µm
25 µm
10 µm
-1.0
-1.2
-1.4
-1.6
Height [m]
2.2
2.4
2.6
2.8
3.0
Major radius [m]

Figure 4.